CHAPTER 4 MICROSTRUCTURE AND MECHANICAL PROPERTIES

4.1 Acicular ferrite

4.1.1 Nucleation and growth of acicular ferrite

Microstructures with a significant proportion of acicular ferrite present an optimised combination of mechanical properties if compared with mainly bainitic structures. It is well documented that acicular ferrite formation is enhanced by the presence of non-metallic inclusions in studies in weld pools[51-64], low carbon steels[65] and medium carbon forging steels[66-69], and is characterized by elongated grains that are "chaotically" arranged[4]. These second-phase particles act as point sites on which the intragranular nucleation[70,71] of ferrite units develops. There may also be some M/A islands present with a high dislocation density[11]. Acicular ferrite is a non-equiaxed structure phase with an interior that contains a dense substructure of dislocations[4,72]. The carbon content in the M/A islands is higher than that in the surrounding matrix. Accordingly, the M/A islands are carbon-enriched, whose formation may be attributed to the partitioning of carbon during the transformation to acicular ferrite and the post-transformation of carbon-enriched austenite. When the specimen is deformed in the non-recrystallisation austenite region, high densities of substructure and dislocations will be formed in the austenite, which increase the nucleation rate of acicular ferrite, impedes the growth of the coherent and/or semi-coherent γ/α interfaces and accelerates diffusion of carbon to these γ/α interfaces, which leads to carbon-enriched austenite. During the accelerated cooling after finish rolling and followed by the coiling process, part of the carbon-enriched austenite transforms to martensite and the retained austenite coexists with the martensite[73]. The transformation model is, therefore, a mix of diffusion and shear transformation[4,9,11,43]. The start temperature of the transformation to acicular ferrite is slightly higher than that of an upper bainite[4,11].

Acicular ferrite always has an orientation relationship with the austenite grain, such

that one of its close packed $\{110\}_{AF}$ planes is nearly parallel to the close-packed $\{111\}_{\gamma}$ plane of the parent austenite. Within these parallel planes, a close-packed $<11\bar{1}>_{AF}$ direction of the acicular ferrite is found to be near to a close-packed $<\bar{1}01>_{\gamma}$ direction of the austenite[74]. This demonstrates that the growth of acicular ferrite occurs by a displacive transformation and its growth, therefore, takes place without carbon diffusion. The excess carbon in ferrite is probably rejected into the austenite soon after nucleation. Acicular ferrite plates are never found to grow across austenite grain boundaries and this is also consistent with the displacive transformation mechanism, since the necessary co-ordinated movements cannot be sustained across austenite grain boundaries. TEM work has revealed that the ferrite units belonging to the same sheaf have the same crystallographic orientation in most cases[75].

As regards the carbon concentration of acicular ferrite structures during transformation, experiments and thermodynamic theory have demonstrated that the growth of acicular ferrite is diffusionless with the ferrite inheriting the chemical composition of the parent austenite. The excess carbon in the acicular ferrite is rejected into the retained austenite after transformation and can apparently occur within a few seconds[74].

4.1.2 Two types of acicular ferrites: Upper and lower acicular ferrite

There are two different microstructural morphologies of acicular ferrite (AF) in medium carbon micro-alloyed steels, depending on the isothermal treatment temperature[75]. One is upper acicular ferrite, the typical acicular ferrite with an interlocked microstructure (plate morphology) that is formed at high isothermal treatment temperatures of typically 450 ºC. The secondary, is of acicular plates of ferrite that had nucleated at the interface between the primary ones and the austenite and are inclined at a high angle with respect to the substrate unit.

Another sheaf morphology of lower acicular ferrite, is composed of packets of plates

following the same growth direction at lower isothermal treatment temperatures of typically 400 ºC. A significant change in the morphology of the acicular ferrite is, therefore, clearly apparent with a lowering of the formation temperature. It is observed that the nucleation of the primary plates takes place intragranularly on the same second-phase particles. These significant differences between the morphologies of the two types of acicular ferrite can be distinguished in the early stages of the transformation. At a high nucleation temperature of 450 ºC, single plates form at second phase particles while at temperatures lower than 400 ºC, individual parallel platelets are formed with residual phases in between them.

There may be two reasons for the formation of parallel AF units at low temperatures. Firstly, the lower stability of the austenite close to the tip of the ferrite plate and secondly, the strain field produced by the invariant plane-strain shape transformation, both favour the formation of the same variant as that of the primary plate at these sites. Further growth of these subunits seems to be possible parallel to the primary plate, leaving a thin layer of carbon-enriched retained austenite between the different subunits. Afterwards, these regions of austenite lead to the precipitation of interlath cementite between the ferrite plates[75].

The autocatalytic formation of new plates of acicular ferrite is expected to depend strongly on the carbon concentration profile of the parent austenite ahead of the interface with the primary AF plates. This concentration profile will become more pronounced as the transformation temperature decreases and the diffusion in the austenite of the carbon rejected from the ferrite, becomes slower. Close to the acicular ferrite tips, the carbon enrichment of the austenite could be low enough to allow the transformation to proceed, leading to the formation of elongated sheaves. At high transformation temperatures, the diffusion of carbon is more rapid and plate formation on interfaces is more likely[75].

4.1.3 Effect of the hot rolling process on acicular ferrite formation

Hot deformation will promote the subsequent formation of acicular ferrite. This is because high densities of substructure and dislocations are formed in the austenite during deformation of austenite in the non-recrystallisation region, which increases the nucleation sites for acicular ferrite and promotes the acicular ferrite transformation[4]. The temperature range for the nucleation of acicular ferrite moves slightly towards higher temperatures and shorter times with hot deformation of austenite if compared to an equivalent austenite without hot deformation. The growth of acicular ferrite, however, is retarded in plastically deformed austenite[76]. With an increase in the cooling rate after hot rolling, the fraction of polygonal ferrite decreases and the fraction of acicular ferrite increases in volume and the grain size of the ferrite becomes smaller[73].

4.2 Acicular ferrite and bainite

Bainite forms typically at temperatures between pearlite and martensite and the transformation model is also a displacive mechanism. There are three kinds of microstructure: upper bainite, lower bainite and granular bainite. Carbides precipitate in-between the laths within upper bainite (which often results in a lower toughness), while carbides are finely distributed within the bainite sheaths at a fixed orientation within lower bainite together with some minor interlath formation of carbides also here. Both forms of carbides have a specific orientation relationship between the bainite lath and the carbides in lower bainite[11].

Bainitic ferrite is very different from acicular ferrite in its shape. It possesses largely parallel sheaves of ferrite with a lath-like structure with some granule-like or rod-like cementite particles alongside or within the laths and along the prior austenite grain boundary network that can be seen clearly. The ferrite in bainite nucleates at the austenite grain boundaries[66,77-80], forming sheaves of parallel plates with the same

crystallographic orientation with respect to the parent austenite. Interlath carbide particles in upper bainite precipitate from the carbon-enriched retained austenite trapped in-between the platelets, or in the lower bainite, from within the supersaturated ferrite within the bainite lath[74].

Acicular ferrite micrographs, on the other hand, have been studied[81] in which the acicular ferrite transformation starts through the nucleation of the primary plates at non-metallic inclusion particles[33,52,54,56,82,84] and progresses by the formation of a new generation of secondary plates of ferrite nucleated at the interfaces of the austenite/AF primary plates[78]. Therefore, inclusions play an important role in the formation of acicular ferrite in low alloy welded metals[85,86] because they provide preferential sites for the nucleation[87-89] of the AF. The acicular ferrite matrix is characterized by a fine non-equiaxed ferrite or interwoven nonparallel ferrite laths[66,73,78,90], which have various sizes distributed in a random manner, very often described as a "chaotic arrangement" of plates showing fine-grained interlocking morphologies[78]. The prior austenite grain boundary network is completely eliminated and some fine M/A island constituents are scattered throughout the matrix[4]. This is due to the partitioning of carbon near the austenite/ferrite interface during the growth of acicular ferrite. The carbon content in the austenite will be increased and accordingly, the austenite's stability will be increased. As a result, the partial austenite that is carbon-enriched, remains and transforms to martensite during the subsequent cooling process, resulting in the M/A island constituent.

4.3 Mechanical properties of line pipe steel

4.3.1 The ratio of yield strength to ultimate tensile strength (YS/UTS)

A low YS/UTS ratio a very important parameter in the API specifications for line pipe steels as a high work hardening rate is required for this application. The lack of strain hardening in high YS/UTS steels means that there is a reduced potential for strain redistribution in thinned areas (thinned by corrosion or weld dressing) during service.

A high strength is, of course, required for line pipe to transport oil or natural gas at higher pressures. The American Petroleum Institute (API) specifies a YS/UTS ratio not greater than 0.93 for an application involving pipelines. The 11 mm line pipe strip steel currently produced by MITTAL Steel (South Africa) tends to have a slightly high YS/UTS ratio of typically 0.93. This ratio is affected by the microstructure of the steel and an optimised microstructure (such as acicular ferrite[32]) is, therefore, beneficial in achieving a lower YS/UTS ratio by carefully controlling the hot rolling, cooling and coiling schedules. This ratio is also an important issue in the development of higher grades of line pipe steels. The specification of line pipe steels of the America Petroleum Institute (API) is shown in table 4.1.

Table.4.1 Specification of line pipe steels of API[12]

Grades of steels	Minimum yield strength (MPa)	Minimum tensile strength (MPa)	Minimum Elongation (%)	Maximum YS/UTS
X65	448	530	20.5	0.93
X70	482	565	19	0.93
X80	551	620	17.5	0.93
X90	601	650	17.5	0.93

Some results showed that there is a slightly higher volume fraction of about 7% of martensite/austenite (M/A) constituent with a higher finish rolling temperature and, therefore, a more rounded stress-strain curve and a higher strain-hardening rate on this curve[1]. It is beneficial to lower the YS/UTS ratio and that author found that when the finish rolling temperature was 720 ºC the ratio was 0.69 and at 780 ºC, the YS/UTS was 0.65 and the volume fractions of M/A constituents were 4.6 and 7.0% respectively for a steel with composition 0.057% C, 0.27% Si, 2.04% Mn, 0.040% Nb, 0.112% Ti and 0.001% B[1].

4.3.2 Toughness

The Charpy toughness specification for the control of fracture initiation normally does not prove too onerous a requirement for higher grade line pipe. Toughness is also important for line pipe steels. Higher toughness can be obtained by lowering the carbon content and refining the ferrite grain size[38]. Niobium can improved Charpy toughness[25,26] at lower finishing temperature below 980 ºC[91]. A lower vanadium content is also useful to increase the toughness[38]. Acicular ferrite microstructures resulted in an improvement of the Charpy toughness with no deterioration of the strength[65,92] whereas bainite resulted poor toughness[66].

4.3.3 U-O pipe forming and Bauschinger effect

During U-O pipe forming, the plate materials are subjected to different cyclic strains, depending on the location along the circumference and in the wall. Typical examples of cyclic strain at locations 180˚ and 30˚ from the longitudinal seam are illustrated in figure 4.1[93].

At the 180˚ location where mill tensile test specimens are usually taken, the outer layer receives a tensile force during U-bending, a compressive force during O-bending, a compressive force during shrinking, and a tensile force during expansion. At the same time, the inner layer is subjected to a cyclic strain of compression, tension, compression and tension.

The total process from U-bending to expansion is not a simple work-hardening process but is actually very complex. On the other hand, during the flattening of a curved pipe section for tensile specimens, the Bauschinger effect and work hardening occur in the outer and inner layer respectively.

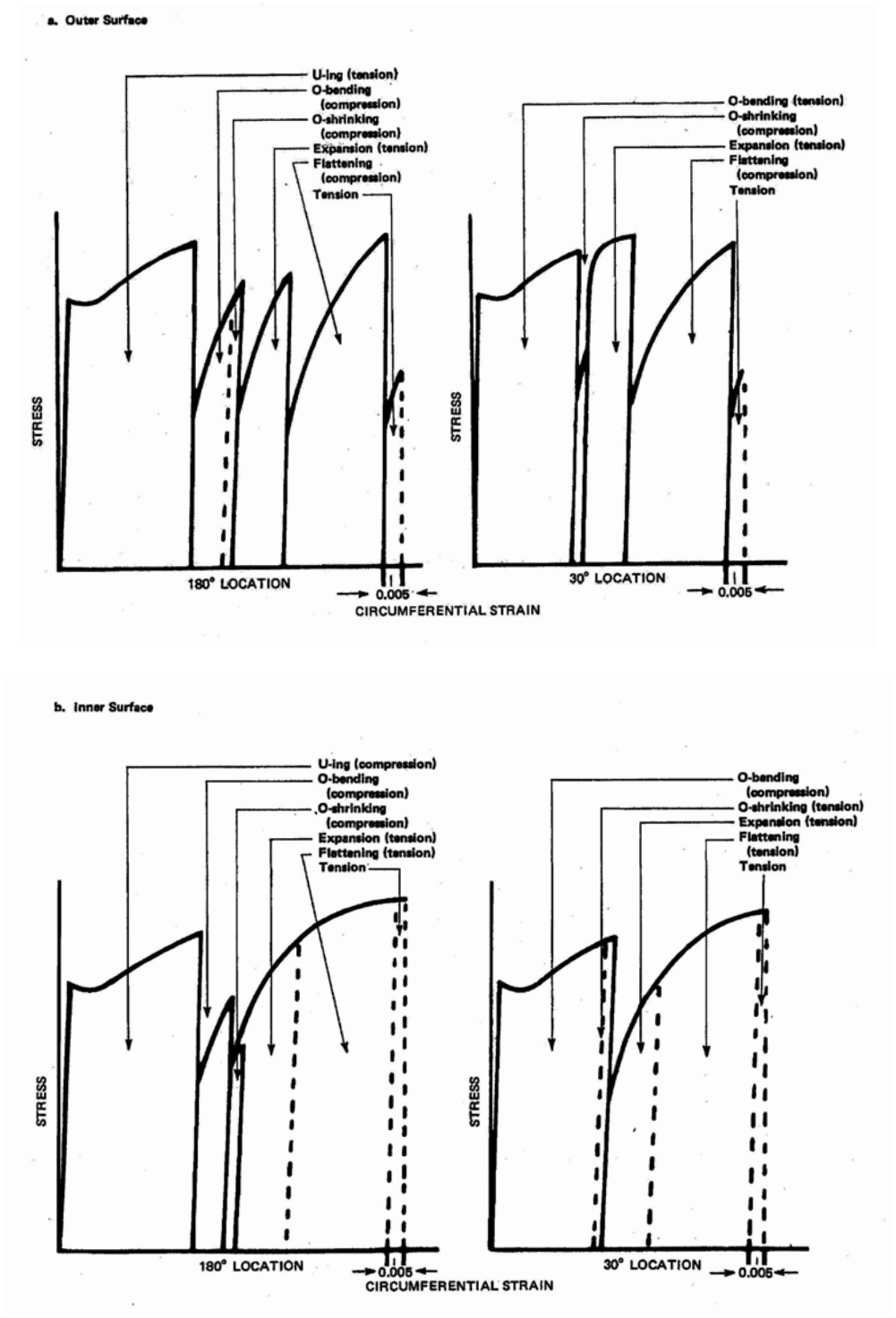

Figure 4.1 Schematic stress-strain curves for the outer (top) and inner (bottom) material during the U-O pipe forming process, with (left) at 180º and (right) at 30º from the welding line[93].

The Bauschinger effect is a characteristic material behavior that is highly dependent on testing conditions[94]. It results in the lowering of a proof-stress value after a

previous single uniaxial initial loading in the opposite direction. When hot rolled strip is converted into ERW line pipe, the pipe forming and sizing strains can significantly modify the pipe yield strength by virtue of the Bauschinger phenomenon. Various steels have different responses to the Bauschinger effect due to different stress-strain curves. Steels with a yield plateau have a Bauschinger strain equal to that corresponding to the strain equal to the yield elongation[95].

The Bauschinger effect is largely controlled by the carbon content and, to a considerably smaller degree, by the manganese content (figure 4.2). Grain size appears to have a minor influence, while the influence of residual-stress conditions is strong (figure 4.3)[94].

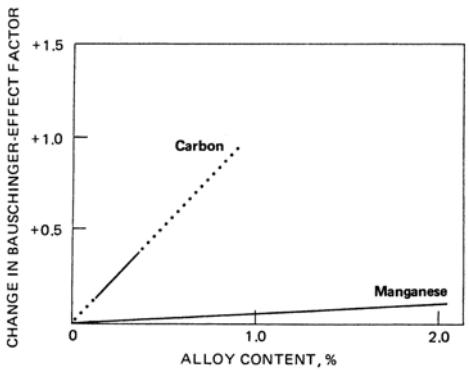

Figure 4.2 The change of the Bauschinger effect factor with carbon and manganese content[94].

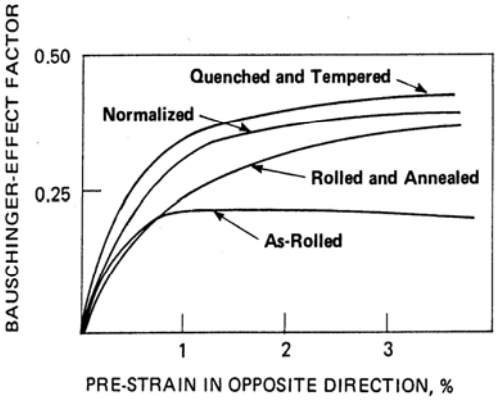

Figure 4.3 The Bauschinger effect in micro-alloyed steel. The upper two curves are for steels with 0.2% C, 0.4% Mn, unalloyed or alloyed respectively with Al, V or Nb. The lower two curves are for low-pearlite steels with less than 0.1% C, 2% Mn, and alloyed with Mo, Nb and Ti[94].

Work-hardening and the Bauschinger effect occur during the pipe-forming process and during the flattening of the tensile test pieces before the tensile test. In the pipe-forming process, work hardening by pipe expansion is more important than the Bauschinger effect, while the reverse is true during sample flattening. The ring-expansion test is used in measuring work hardening. The pipe after forming, has a considerably higher yield strength than the plate, which indicates that work hardening has taken place during pipe forming[96].

CHAPTER 5 BACKGROUND OF CURRENT SOUTH AFRICA LINE PIPE PRODUCTION

5.1 Line pipe steel composition of Mittal Steel (South Africa)

The chemical composition of the current Mittal Steel (SA) line pipe steel is provided in table 5.1.

Table 5.1 Typical chemical composition of the current 11 mm line pipe steel of Mittal Steel, (wt%)

C	Si	Mn	P	S	Cr	Ni	Mo	Cu	Al
0.066	0.258	1.583	0.011	0.004	0.021	0.007	0.001	0.007	0.037

V	Nb	Ti	Sn	B
0.062	0.037	0.017	0.001	0.0002

5.2 Parameters of the hot rolling process at Mittal Steel (SA)

The parameters of hot rolling of line pipe steels at Mittal Steel are shown in table 5.2.

Table 5.2 The parameters of the hot rolling process at Mittal Steel

Pass No		Reheating temperature, °C)	R1	R2	R3	R4	R5	R6	F1	F2	F3	F4	F5	F6
Force (tons)									1860	1552		1150	1076	1053
Temperature (°C)	in	1200	1150						1042	1008		938	915	896
	out							1050	1008	969		915	896	879
Gauges (mm)	in		240	195	160	120	85	60	40	28.87		21.02	15.76	13.51
	out		195	160	120	85	60	40	28.87	21.02		15.76	13.51	11.70
Strain/pass, ε			0.21	0.20	0.29	0.34	0.35	0.40	0.32	0.32		0.29	0.15	0.14
Total strain			1.79						1.22					
Strain rate (s^{-1})									9.4	16.1		22.6	20.9	26.2
Roll speed, V (ms^{-1})				~1.5	~1.5	~1.5	~1.5	~1.5		1.8		2.7	3.3	3.9
Inter-pass time, t, (s)				10	10	10	10	10		2.7	1.8	1	1.5	1.3
Inter-pass cooling rate (°Cs^{-1})				3	3	3	3	3						
Cooling rate after finishing (°Cs^{-1})			40 °Cs^{-1} —for 6mm of the final thickness of strip 20 °Cs^{-1} —for 11.5mm 50 °Cs^{-1} —for 5mm											
t/D (Thickness/Diameter)			~2.4%											

NB: F3-dummy for rolling

5.3 Typical microstructures and existing developments within Mittal Steel for line pipe steel

The optical microstructure of the current 11 mm wall thickness line pipe steel for Mittal Steel is shown in figure 5.1. This is the alloy that was used for a major part of the pipe-line for large-scale gas transportation from Mozambique to Secunda in a 2.5 meters diameter pipe line. The microstructure is a mixture of polygonal ferrite, acicular ferrite and pearlite.

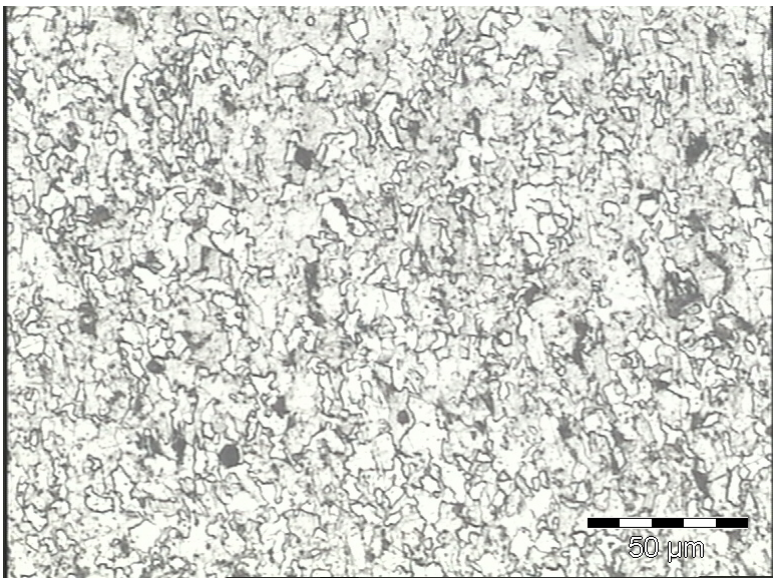

Figure 5.1 The optical microstructure of cast #521031, Mittal Steel line pipe

Smaller thin walled (about 6 mm thickness) pipelines may be used in future within South Africa for smaller scale gas distribution and reticulation to consumers. The current steel produced by Mittal Steel tends to have a slightly high YS/UTS ratio of 0.93, which is on the maximum limit of the specification of the American Petroleum Institute (API) of 0.93 for an application involving pipelines. The current line pipe steel consists typically of about 0.06% carbon with micro-alloying elements of titanium, niobium and vanadium (generally less than 0.05% for each) and is produced either via the Electric Arc Furnace (EAF) or Basic Oxygen Furnace (BOF) route.

5.4 The hypothesis for this study

The objective of this study is to establish the relationship between micro-alloying elements, the microstructure and deformation in austenite on the ratio of YS/UTS and other mechanical properties. Therefore, a study is to be undertaken on the austenite to acicular ferrite transformation with particular emphasis on the kinetics of the acicular ferrite formation and as affected by the above process variables. The experimental research would include a redesign of the chemical composition, dilatometer analyses, simulation of the controlled rolling process on a Gleeble 1500 (initially the work was started on a Gleeble 1500^{TM} model but halfway through the study, the Gleeble was upgraded to a Gleeble 1500^{D} DSI), microstructural observations, tensile tests, SEM and TEM investigations, etc.

5.4.1 Design of the chemical compositions of the investigated alloys

The V-content in the steel was decreased in this study because it only contributes to dispersion hardening as V(C,N) in ferrite. Its dispersion hardening is less than that of Nb in steels.

Niobium is a very important micro-alloying element in line pipe steels and formed one of the main-alloying elements considered in this study. It contributes to dispersion hardening (NbC in ferrite), promotes acicular ferrite formation (reduction of pearlite) and raises the T_{nr} (“pancake” of austenite). The niobium concentration was increased to about 0.045%wt (which is more than the 0.037% used currently by Mittal Steel).

Titanium is another micro-alloying element that retards austenite grain growth during reheating. The reheating temperature may be as high as 1225 ºC due to undissolved TiN. If titanium binds the free nitrogen in the steel, more niobium will be available in the ferrite to precipitate as NbC and will increase the precipitation hardening. Titanium can also control the shape of sulphide inclusions (TiS). Accordingly, the titanium addition was kept at levels of 0.017 to 0.022% in this study.

Molybdenum contributes to phase transformation hardening and can be used instead of V in the hardening of steels. It might benefit the increase in volume fraction of acicular ferrite and M/A islands that are useful to lower the ratio of YS to UTS. Molybdenum can diminish the Bauschinger effect during pipe forming. Thus, molybdenum was added to the experimental alloys in this study. The molybdenum additions considered here were 0.10%, 0.15% and 0.25%, respectively.

Carbon was slightly decreased to 0.05% C in this study for the purpose of improving the weldability of steel.

Summarising the target analysis above, the chemical compositions of the experimental alloys were designed as follows (Table 5.3):

Table 5.3 Design of chemical composition ranges of alloys that were investigated (in wt%)

C	Si	Mn	S	P	V	Nb	Ti
0.05	0.2-0.25	1.0-1.2	<0.005	<0.01	0	0.045	0.022

N	Cu	Ni	Al	Cr	Ca	Mo
0.006	0.007	0.007	0.03	0.02	0.002	0.1-0.25

5.4.2 Design of the controlled hot rolling process

The austenite grain size of the current Mittal Steel alloy, reference alloy #6 (Mo-free) was found to be 57 and 63 μm at 1225 ºC for 60 and 120 minutes respectively. Therefore, the reheating temperature of 1225 ºC was chosen for this study to provide almost complete dissolution of the niobium carbonitrides to achieve maximum precipitation hardening, but little austenite grain size coarsening.

In this study, the finish rolling temperature was maintained at about 870 ºC, i.e. above the A_{r3} and, therefore, with no deformation in the (α+γ) two-phase region.

The temperature range for rough rolling was chosen to be from about 1190 to 1000 ºC in this study, which is above the non-recrystallisation temperature T_{nr}. The total or cumulative true strain in the rough rolling stage was chosen to be about 1.4 with individual pass strains of more than 0.2.

The final temperature for the finish rolling stage was between 840 to 870 ºC. The finish rolling temperature in this stage was maintained above the A_{r3} temperature. The deformation for this stage was, therefore, carried out in the austenite non-recrystallisation region. The total strain in the finish rolling stage was about 0.54 in order to accumulate enough rolling strain within the austenite grains for the subsequent ferrite transformation, leading to a pass strain of more than 0.2 as well.

The initial and final thicknesses of the ingot and plate for laboratory hot rolling were planned to be 43 and 6 mm respectively, with a total heavy reduction of 86%.

The cooling rate after finish rolling has a significant effect on the subsequent microstructure of the line pipe steel. Rapid cooling is useful to increase the volume fraction of acicular ferrite and this contributes to good mechanical properties. It results in a continuous stress-strain curve, decreases the Bauschinger effect during pipe-forming and leads to a low ratio of YS/UTS. In this study, various cooling rates and with/without prior deformation in the austenite on the Gleeble were used to establish the effect of these parameters on the ratio of YS/UTS. For this purpose, the experimental challenge was how to measure the volume fraction of acicular ferrite?

The coiling temperature is also very important to the degree of precipitation hardening of line pipe steels. If the coiling temperature is too high, the precipitates become too

coarse. At low temperatures acicular ferrite may form, but the temperature cannot be too low because the precipitation requires diffusion, and in this study two coiling temperatures of 600 and 575 ºC were chosen. These are also the previous and the current coiling temperatures respectively used by Mittal Steel in their 11 mm strip steel for line pipe.

In this study a hypothesis that the acicular ferrite or an optimised mixture of acicular ferrite and polygonal ferrite, is the most suitable microstructure for decreasing the ratio of YS/UTS of steels, was, therefore, tested.

A series of tests on the Gleeble were also carried out to study the effect of cooling rate, coiling temperatures and deformation prior to transformation on the ratio of yield strength to ultimate tensile strength.

CHAPTER 6 EXPERIMENTAL PROCEDURES

This chapter describes the experimental procedures for the investigation, including the alloy design, the melting and casting of the ingots, the hot-rolling process, the testing of the austenite grain size and the presence and identification of undissolved particles, the determination of the non-recrystallisation temperature, the determination of the strain-free and the strain affected CCT diagrams and the determination of the mechanical properties, etc. Distinguishing between the acicular ferrite and polygonal ferrite in the microstructures of the samples was done by TEM through shadowed carbon extraction replicas and thin foils. The chemical compositions of the experimental alloys were typical of commercial line pipe steels with Nb-V-Ti micro-alloying elements with the current line pipe steel from Mittal Steel as the reference steel.

6.1 Alloy design

As indicated earlier and briefly summarised here again, the design of the experimental alloys was based on the considerations set out below.

1. The chemical compositions of HSLA line pipe steels are normally low in carbon and contain some micro-alloying elements that may be only one, or a combination of any two or three of the micro-additions (vanadium, niobium and titanium). A low carbon level was selected for improving the weldability and toughness, to provide less pearlite and more effective dissolution of niobium during reheating that will increase the precipitation hardening of these steels.
2. Niobium has strong dispersion hardening characteristics due to the formation of NbC in ferrite. It promotes the transformation to acicular ferrite that can be beneficial to lower the ratio of yield strength to ultimate tensile strength of these steels. Niobium also causes refinement of the austenite grains during the rolling process by raising the non-recrystallisation temperature (T_{nr}). Accordingly, a little more niobium was considered than in the current Mittal Steel alloy while

vanadium was reduced or left out, which decreases the non-recrystallisation temperature.

3. Titanium can retard the austenite grain growth during reheating of slabs due to the presence of TiN particles. As described above, considering the stoichiometric ratio of Ti to N (3.4 /1) and preventing MnS stringer inclusions, (which requires Ti/S in TiS of 1.5/1), the ideal titanium addition was calculated from equation (2.1).
4. The addition of molybdenum in Nb-containing steels can improve transformation hardening (increased volume fraction of acicular ferrite and M/A islands), can provide grain refinement and precipitation hardening. It also greatly suppresses or delays the formation of polygonal ferrite and pearlite[4]. Additions of molybdenum were, therefore, considered instead of the usual vanadium for enhancing the strength of the steels. In steels with molybdenum, the stress-strain curve of the as-rolled plate is usually continuous, without an upper yield points[33]. This may provide control of the Bauschinger effect and contribute to an increase in yield strength from plate to pipe.

Thus, the newly designed alloys that were made up, all had the same low carbon, niobium and titanium levels but were made with and without vanadium, and also had varying amounts of molybdenum.

6.2 The melting of the experimental alloys

Sections from the currently produced line pipe steel from Mittal Steel were used as feed stock material for the melting of the new alloys in a 50 kg vacuum induction melting furnace at Mintek. The liquid steel was cast into ingots of 43 × 66 × 235 mm. The chemical compositions of the five new alloys are listed in table 6.1. The Mittal Steel line pipe steel is included in the table as a reference.

Table 6.1 Chemical compositions of the experimental alloys, in wt.%

Alloy #	C	Si	Mn	P	S	Cr	Ni	Mo
1	0.05	0.29	1.21	0.014	0.011	0.07	0.07	0.01
2	0.06	0.25	1.29	0.018	0.01	0.05	0.04	0.09
3	0.05	0.23	1.05	0.019	0.011	0.04	0.04	0.09
4	0.05	0.24	1.31	0.019	0.011	0.05	0.04	0.12
5	0.05	0.25	1.14	0.019	0.011	0.05	0.04	0.22
6(Mittal Steel)	0.066	0.26	1.583	0.011	0.004	0.021	0.007	0.001

Cu	Al	Co	V	Nb	Ti	Sn	B	Free-N
0.02	0.004	0.006	0.06	0.055	0.017	--	0.0001	0.0068
0.03	0.055	0.009	<0.005	0.05	0.019	0.003	0.0003	0.0035
0.03	0.054	0.008	<0.005	0.051	0.019	0.003	0.0002	0.0032
0.02	0.055	0.009	<0.005	0.052	0.019	0.003	0.0003	0.0032
0.02	0.065	0.01	<0.005	0.055	0.021	0.003	0.0003	0.0027
0.007	0.037	--	0.062	0.037	0.017	0.001	0.0002	--

6.3 The effect of reheating temperature and soaking time on the austenite grain sizes

The samples from the cast ingots were machined into cubes of about 10 × 10 × 10 mm. Two methods were used to process these samples in order to measure the austenite grain size. The first was to reheat the samples at temperatures of 1150, 1200, 1225 and 1250 °C, respectively, and then quench them into water. The samples were etched using many different etchants (see table 6.2), but the results revealed that these etchants were not suitable to reveal the prior austenite grain boundaries for the alloys studied. The carbon content of the alloys was probably too low for this. The more successful technique was a modified McQuaid-Ehn method by carburising the samples after reheating in argon, in-situ within the austenite region in a dry carbon monoxide gas atmosphere at 927 ºC for up to 5 hours directly after reheating at the above four austenitisation temperatures, i.e. without going through the ferrite transformation. Pro-eutectoid cementite formed on the prior austenite grain boundaries during very slow cooling from the carburisation temperature at 927 ºC down to 690 ºC at which temperature the sample was removed from the furnace. Thus,

the cementite layers indicated the sites of the original austenite grain boundaries, which then became easy to measure. The carburising process is illustrated in figure 6.1. After carburisation, the samples were polished and etched in a 2% Nital solution and then the original austenite grain sizes were measured by the mean linear intercept method[97].

Table 6.2 The composition of the etchant solutions

Solution Number	**Chemical**	**Quantity**
#1	Picric acid	1 g
	Hydrochloric acid	5 ml
	Ethanol alcohol	95%
#2	$FeCl_3$	1 g
	H_2O	100 ml
#3	$FeCl_3$	1 g
	Hydrochloric acid	5 drops
	H_2O	100 ml
#4	Sodium bisulphite	34 g
	H_2O	100 ml
#5	Hydrochloric acid	40 ml
	Sulphuric acid	10 ml
	H_2O	50 ml
#6	10% aq. Oxalic acid	28 ml
	H_2O_2(30%)	4 ml
	H_2O	80 ml

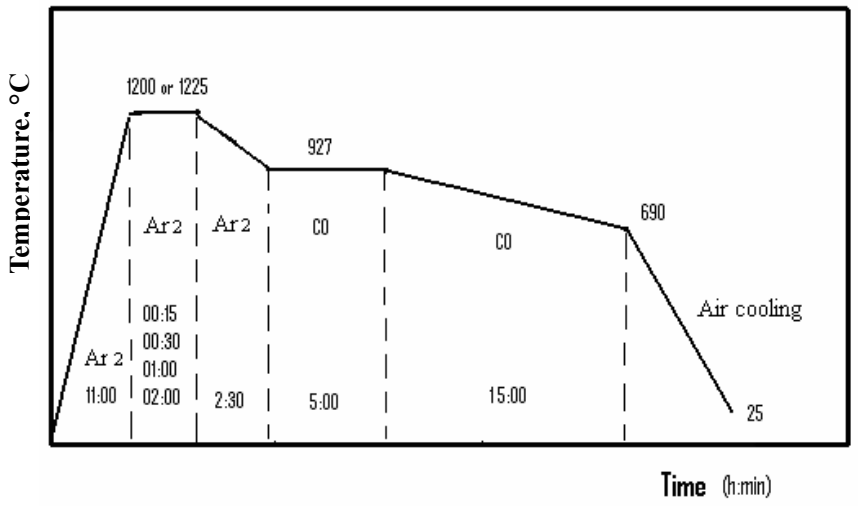

Figure 6.1 Schematic of the modified McQuaid-Ehn carburising process of the samples directly after reheating.

6.4 Measuring the presence and composition of undissolved particles

During reheating, any undissolved small particles will retard the austenite grain growth. Before entering the first rough rolling pass, a fine austenite grain size is beneficial to the later strength and toughness of the steels. The quantity and the size of the undissolved particles are related to the reheating temperature. Austenitisation temperatures ranging from 1150 to 1250 °C were employed, together with soaking times of 15 to 120 minutes for this part of the investigation. The samples were quenched into water or were fast cooled in helium gas. The details of these treatments are listed in table 6.3 below. The samples were mechanically ground and polished after the treatment, then were lightly etched in a 2% Nital solution without an apparent visible optical microstructure of the matrix, and vacuum coated with carbon. The shadowed carbon extraction replicas were similarly made, also after light etching in 2% Nital, then the vacuum application of Au-Pd shadowing at an angle between 20 to 40º before vertical coating of the carbon. The size of the particles was measured on the micrographs obtained from the transmission electron microscope (TEM) and their volume fraction calculated using the following equation[98]:

$$f = \frac{\pi}{6} N_s (\overline{\chi}_{Al}^2 + \sigma_{Al}^2) \qquad (6.1)$$

$$\sigma_{Al}^2 = \frac{n\Sigma x_{Al}^2 - (\Sigma x_{Al})^2}{n(n-1)} \quad (6.2)$$

where $\overline{x}_{Al}$ is the planar arithmetic mean of the particle diameter;

f is the volume fraction of particles;

N_s is the total number of particles intersecting a unit area;

σ_{Al}^2 is the standard deviation of the particle size distribution;

x_{Al} is the diameter of a particle;

n is the total number of particles measured.

Table 6.3 Temperatures and soaking time of the treatment for undissolved particles

Temperature (ºC)	**Time (min)**		
1150	15	60	120
1200	15	60	120
1225	15	60	120
1250	15	60	120

6.5 Non-recrystallisation temperature (T_{nr})

The finishing temperature of rough rolling is associated with the non-recrystallisation temperature (T_{nr}) and heavy reductions must take place within this recrystallisation region at temperatures higher than the T_{nr} in order to obtain a fine recrystallised austenite grain size at the start of finish rolling below the T_{nr}. This is beneficial to high strength and good toughness of the steels. Accordingly, the non-recrystallisation temperature is an important parameter that should be considered when the hot rolling process is designed. Many researchers have studied the recrystallisation of austenite[99-107] and some mechanisms have been proposed[108-110]. The

non-recrystallisation temperature may be a function of the parameters[99,111-113] of the rolling process, such as pass strain[114,115], strain rate and inter-pass time[48], and may also depend on the content of micro-alloying elements[116], etc. The hot torsion test has been widely used to simulate industrial hot rolling processes[117-121]. In this study, the recrystallisation behaviour of the steel was investigated during multi-pass compression deformation on a Gleeble hot working facility on cylindrical samples of 8 mm in diameter and 15 mm in length that were machined from the as-cast ingots.

6.5.1 Testing schedule for the determination of the T_{nr}

Reheating temperatures should be high enough to dissolve all the precipitates (mainly the Nb precipitates, but except the TiN) because the micro-alloying elements affect the non-recrystallisation temperature. The reheating temperature for Nb precipitates can be determined from the following equation[122,123]:

$$\log[Nb]\left(C+\frac{12}{14}N\right)=2.26-\frac{6770}{T} \qquad (6.3)$$

The calculated solution temperatures for Nb(C,N) in the experimental alloys are listed in table 6.4.

Table 6.4 Calculation equilibrium Nb carbonitride solution temperature

Alloy number	Solution temperature of Nb(C,N) (ºC)
1	1145
2	1149
3	1179
4	1130
5	1137

Laasraoui[124] reported that the niobium carbonitrides remained undissolved at reheating temperature of 1100 ºC for an 0.04% Nb steel. Thus, a maximum reheating temperature of 1225 ºC was selected here.

Samples of alloy #6 (the current Mo-free Mittal Steel alloy) were heated to 1225 °C at a heating rate of 100 °Cmin^{-1} and held at this temperature for 15 minutes. The multi-pass compression tests were carried out using the test parameters shown in tables 6.5 and 6.6. Pass strains, ranging from 0.15 to 0.32, and inter-pass times ranging from 4 to 50 seconds were employed, at a constant strain rate of 1 s^{-1}. In two particular tests, the inter-pass time and pass strain were held constant. Another test of strain rate ranging from 0.1 to 2.22 s^{-1}, was also employed at a constant pass strain of 0.2 and constant inter-pass time of 8 seconds (see table 6.7). Such a multi-pass compression testing schedule is illustrated schematically in figure 6.2 below.

Table 6.5 Testing parameters for T_{nr} at strain ranging from 0.15 to 0.32

Inter-pass time (s)	8	8	8	8	8	8
Strain rate (s^{-1})	1	1	1	1	1	1
Strain/pass	0.15	0.2	0.24	0.28	0.30	0.32

Table 6.6 Testing parameters for T_{nr} at inter-pass times ranging from 4 to 50 seconds

Inter-pass time (s)	4	6	8	15	20	30	35	40	50
Strain rate (s^{-1})	1	1	1	1	1	1	1	1	1
Strain/pass	0.2	0.2	0.2	0.2	0.2	0.2	0.2	0.2	0.2

Table 6.7 Testing parameters for T_{nr} at strain rate ranging from 0.1 to 2.22 s^{-1}

Inter-pass time (s)	8	8	8	8	8	8	8	8	8
Pass strain, ε	0.2	0.2	0.2	0.2	0.2	0.2	0.2	0.2	0.2
Strain rate (s^{-1})	0.1	0.47	0.9	1.22	1.38	1.67	1.80	2.0	2.22

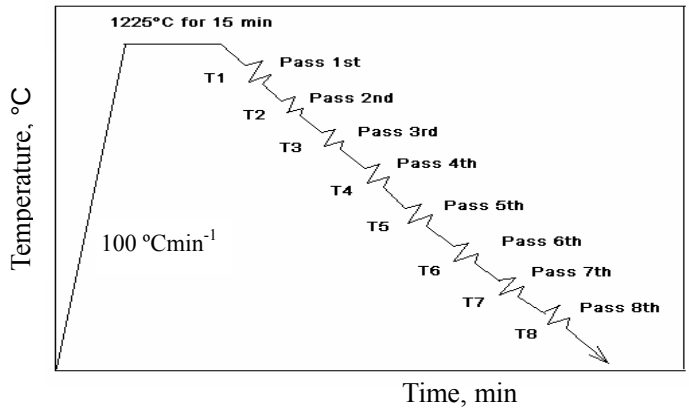

Figure 6.2 Schematic schedule employed in the multi-pass compression tests for the T_{nr}.

6.5.2 The determination of the non-recrystallisation (T_{nr})

A typical set of curves of the true flow stress versus true strain from a multi-pass compression test is illustrated in figure 6.3.

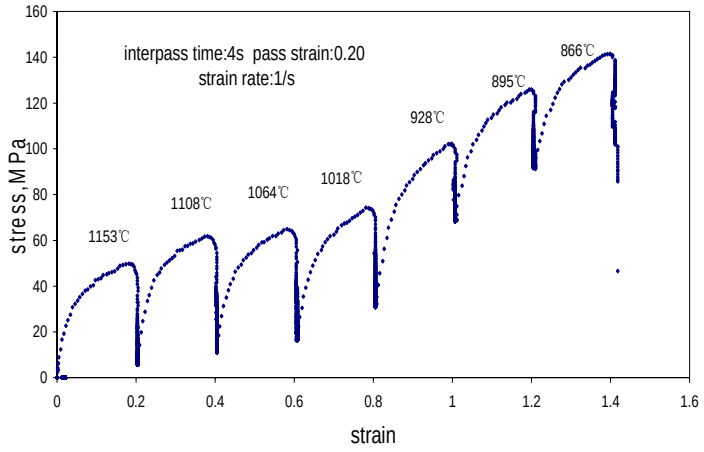

Figure 6.3 The curves of flow stress versus strain in a multi-pass compression test on alloy #6.

The mean flow stress of each pass was calculated from the following equation and the flow stress-strain curve (see figure 6.3):

$$\bar{\sigma} = \frac{1}{\varepsilon_b - \varepsilon_a} \int_{\varepsilon a}^{\varepsilon b} \sigma d\varepsilon \qquad (6.4)$$

The non-recrystallisation temperature was determined from the relationship between the mean flow stress (MFS in MPa) of each pass and the inverse temperature (1/T in K^{-1}) of the compression deformation, as illustrated in figure 6.4. This typical curve is divided into two stages by a slope change in the two straight line sections. In the lower slope stage (which corresponds to a high temperature deformation), full recrystallisation takes place during the pass because there is no strain accumulation and the increase in the mean flow stress is solely due to the decrease in temperature of the inherent strength of a well annealed microstructure. However, in the higher slope stage (deformation below the T_{nr}), there is only partial dynamic recrystallisation, or no recrystallisation at all, indicating that the strain is accumulated from pass to pass, and the mean flow stress increases more rapidly with decreasing temperature[125]. The intersection of two straight lines provides the T_{nr}.

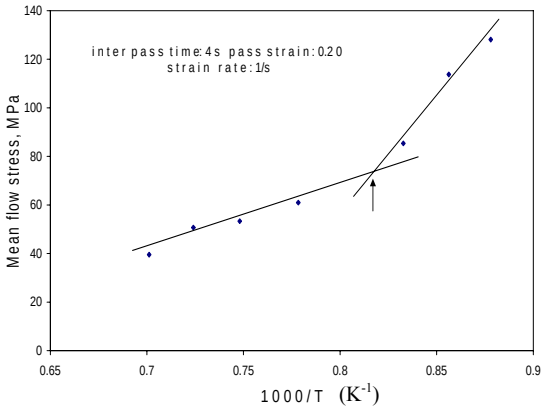

Figure 6.4 Determining T_{nr} from the mean flow stress in MPa versus the inverse pass temperature in K, during a multi-pass compression test on alloy #6.

6.6 CCT-diagram

The alloys used for the CCT diagrams, were the as-cast alloy #5 (with 0.22% Mo) and alloy #6 (Mo-free) (Mitall Steel reference alloy). The chemical compositions of alloys #5 and #6 were listed in table 6.1. Samples of with a size of a 15 to 16 mm long cylinder with a diameter of 7 mm were used for the strain affected CCT tests, and a 8 to 9 mm long cylinder with a diameter of 7 mm for the strain-free CCT test were used. The temperatures of phase transformations were measured by the C-strain facility on the Gleeble which measures the change in diameter of the sample during cooling for the strain affected CCT tests.

6.6.1 The A_{c1} and A_{c3} test

The A_{c1} and A_{c3} are the important critical equilibrium temperatures for starting and completion of the austenitisation transformation during phase transformation of low carbon hypoeutectoid steels (less than 0.77% C). The determination of the A_{c1} and A_{c3} temperatures were made on a single-LVDT THETA dilatometer facility. Phase transformations are normally associated with a non linear volume change in the temperature range of the transformation. The linear thermal expansion or contraction of the samples, therefore, takes place in a manner that allows the subtraction of the linear relationship between dilatometry and temperature from the non-linear transformation portions. A schematic sketch of the dilation with temperature is represented in figure 6.5[126]. Figure 6.6 shows the schematic determination of the A_{c1} and A_{c3} temperatures of steels on the heating curve of dilation versus the testing temperature. In order to completely dissolve all the Nb-alloyed precipitates in this study, e.g. the Nb(C,N), the reheating temperature was chosen as 1225 ºC for 15 minutes with a heating or cooling rate to and from this temperature of 3 ºCmin^{-1} for equilibrium conditions. Samples for the THETA dilatometer were cylinders with a 7 mm diameter and a 10 mm length. The chamber containing the samples was kept at a vacuum of 10^{-4} torr, to prevent any significant oxidation of the samples.

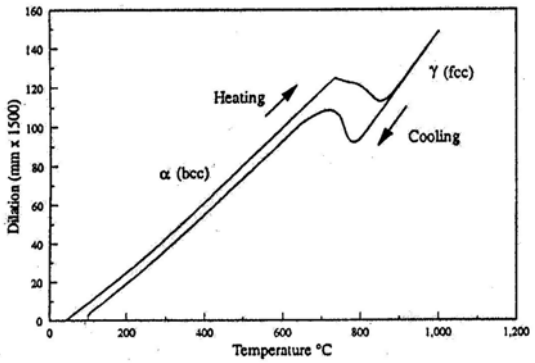

Figure 6.5[126] Schematic dilation as a function of testing temperature.

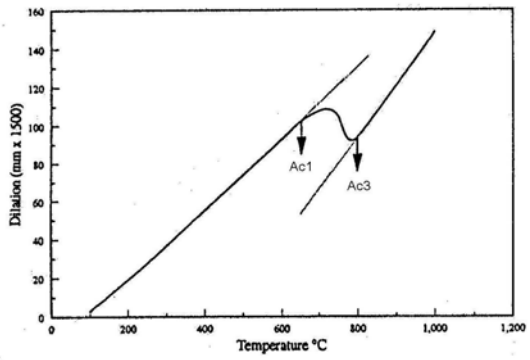

Figure 6.6[126] Schematic determination of the A_{c1} and A_{c3} temperatures on the heating curve.

6.6.2 CCT diagram without prior deformation

The continuous cooling transformation (CCT diagram) without prior deformation was also made on the THETA Dilatometer. The reheating rate was taken as 100 ºCmin^{-1} up to 1225 ºC and held for 15 minutes at this temperature for the purpose of complete dissolution of the Nb-precipitates. The samples were subsequently cooled down to 980 ºC at a rate of 5 ºCs^{-1} and held for 5 minutes at this temperature before finally, cooling down to 25 ºC at the various almost linear cooling rates of 0.1, 0.2, 0.5, 1, 2, 5, 8, 10 and 20 ºCs^{-1}, respectively. The sample chamber was evacuated before cooling after 980 ºC and the cooling media was either flowing argon or helium gas, depending on the required cooling rate. The chamber of the THETA dilatometer and the schematic test schedule are illustrated in figures 6.7 and 6.8, respectively. After cooling, samples were polished and etched in 2% Nital and the microstructures examined with an Olympus PMG3 optical microscope. A combination of the optical micrographs and the cooling curves of dilation with the test temperature, were used to determine the phase transformation temperatures. The CCT diagram was then constructed from the various curves of temperature on a linear scale with the test time on a log scale and the phase transformation temperatures indicated on these.

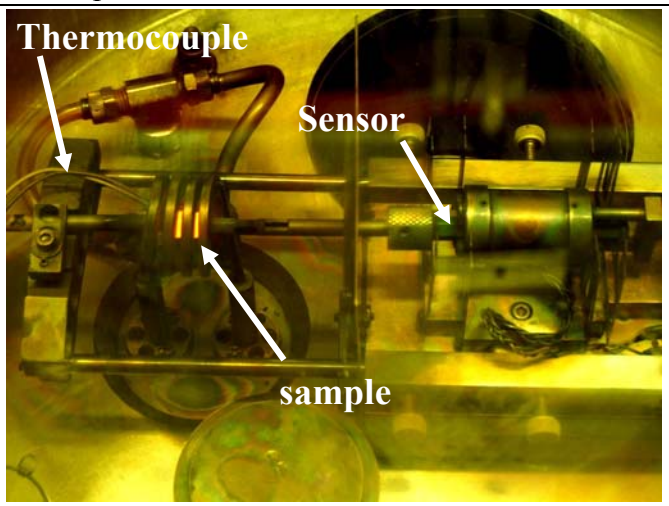

Figure 6.7 Dilatometer chamber

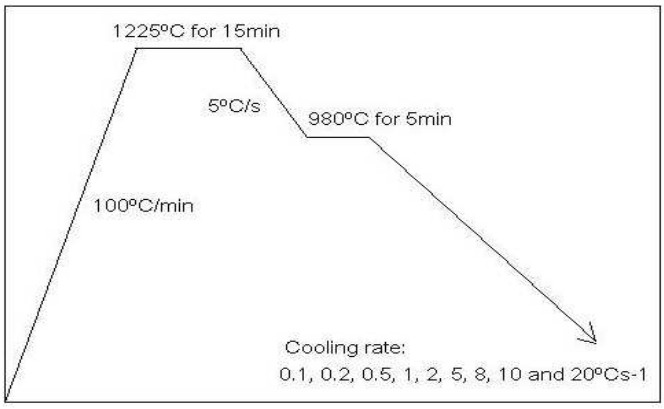

Figure 6.8 Schematic schedule of the test for the CCT diagram on the THETA Dilatometer.

6.6.3 Strain affected CCT diagram

The stain affected CCT diagram with prior deformation, was carried out on Gleeble 1500^{D} DSI hot simulator. The reheating rate was also 100 ºCmin^{-1} up to 1225 ºC and held for 15 minutes at this temperature for the complete dissolution of precipitates in an argon atmosphere. The samples were then cooled down to 860 ºC at 10 ºCs^{-1}, and held for 5 minutes at this temperature. The samples were then compression deformed with a strain of 0.6 (45% reduction below the T_{nr}) at 860 ºC at a strain rate of 0.5 s^{-1}. Samples were finally cooled down to room temperature after deformation, at the various linear cooling rates of 0.1, 0.2, 0.5, 1, 2, 5, 8, 10, 20 and 40 ºCs^{-1}, respectively. The cooling media was also argon (for a slow cooling rate) or helium gas (for a rapid

cooling rate). The steps for preparing the micrographs were the same as for the strain-free CCT diagram above. The chamber of the Gleeble hot simulator and the schematic test schedule are illustrated in figures 6.9 and 6.10, respectively. The C-gauge facility of the Gleeble was used to measure the dilation of the sample during cooling after compression deformation.

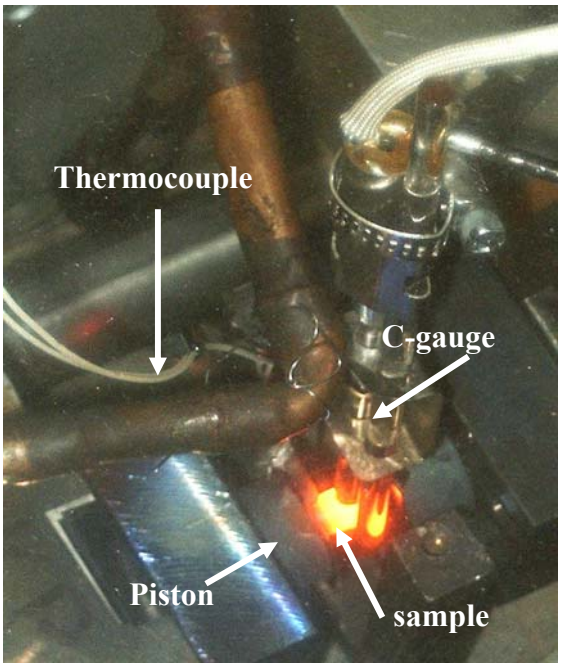

Figure 6.9 Chamber of the Gleeble 1500^{D} DSI

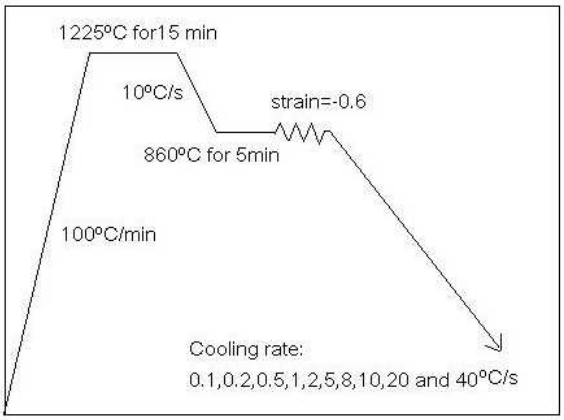

Figure 6.10 Schematic schedule of the test for the strain affected CCT diagrams on the Gleeble.

6.7 The thermo-mechanical process

6.7.1 Cooling unit

A specially constructed cooling unit was used to cool the laboratory melted ingots after hot rolling in a controlled manner. The cooling unit consists of nozzles, a water pump, control valves, and a water box etc. The experimental arrangement is shown in figure 6.11. The coolant is fed with compressed air and sprayed onto the cooling samples through nozzles. The linear distance between the nozzles was about 70 mm, so that uniform cooling of samples of about 100 × 300 mm could be attained. The cooling rate, for instance, was 21 °Cs^{-1} using fresh water at 24 °C as the coolant and with compressed air spraying of the water with an air pressure of 580 MPa. A higher figure of 47 °Cs^{-1} was achieved with a 10% NaCl aqueous solution instead of water.

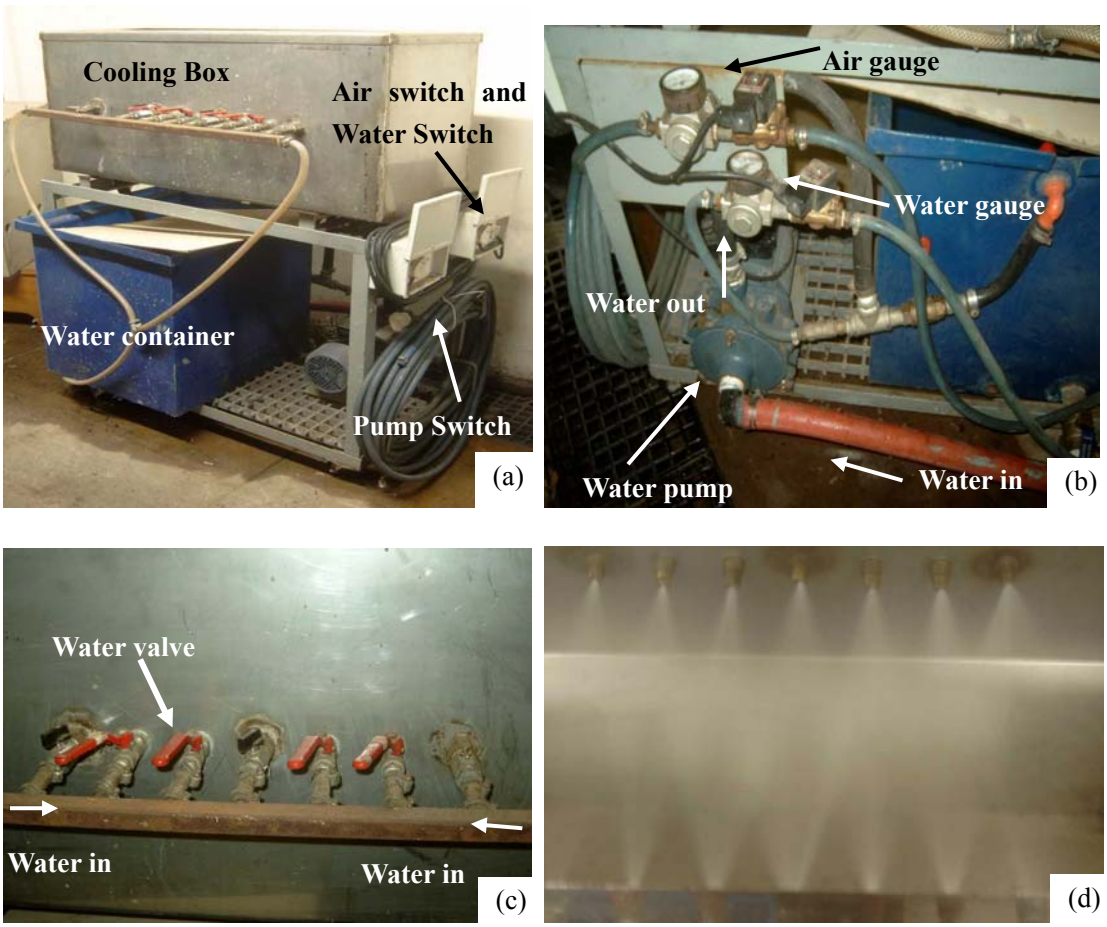

Figure 6.11 Experimental arrangement of the cooling unit for controlled cooling: (a) overall view, (b) controller for mixing of gas and water, (c) valves for the nozzles and, (d) cooling spray in the chamber from the spraying jets.

6.7.2 Hot rolling process of the laboratory ingots

The schedule for the laboratory hot rolling of the ingots, i.e. the pass strain, the total reduction and inter-pass times etc., were controlled as far as possible to optimise the process for austenite grain refinement[114,115]. The experimental casts were hot rolled on a two-stand laboratory hot rolling mill equipped with 10 inch rolls. The ingots of a machined 43 × 90 × 66 mm size for the alloys #1 to #6 were reheated and hot rolled to 6 × 100 × 300 mm plates with the final thickness of 6 mm chosen to simulate a possible future reduced gauge for Mittal Steel from their current 11 mm strip.

6.7.2.1 Reheating before laboratory hot rolling

From the results of the study of the effects of temperature and time on the austenite grain size, a reheating temperature of 1225 °C and a time of 60 minutes were taken. This is quite safe as it has been reported that austenite grains will not coarsen unduly before an austenitisation temperature of about 1250 °C is reached in V-Nb-Ti micro alloyed steels[35].

6.7.2.2 Rough rolling of the laboratory hot rolling

As indicated before, the metallurgical function of roughing is to refine the coarse austenite grains after the reheating and soaking to achieve the finest possible dynamically recrystallised grains before entering the finish rolling below the T_{nr}. Pass strains should, therefore, be at least 0.2 or higher to promote Dynamic Recrystallisation (DRX) during rough rolling to produce finer recrystallised grains. The starting temperature for rough rolling of the laboratory cast ingots was between 1148 and 1190 °C and five passes in this roughing stage were undertaken, with a total roughing strain of 1.43.

6.7.2.3 Finish rolling of the laboratory hot rolling

As before, the objective of this stage is to accumulate sufficient rolling strain within the austenite grains to promote a finer ferrite transformation after rolling. Ferrite nucleation sites are, therefore, greatly multiplied in number and a very fine ferrite grain size can be generated during the subsequent controlled cooling[6]. In this study three passes were used with a total strain of 0.54 and the finish rolling temperature was maintained between 857 and 865 °C.

6.7.2.4 Cooling rate after laboratory finish rolling

The cooling rate (V_c) and the finishing temperature (T_c) of the accelerated cooling after finish rolling, are important parameters of the thermo-mechanically controlled processing for the experimental alloys to achieve their optimum strength and controlling the T_c and V_c may lead to the control of the precipitation of carbonitrides during the accelerated cooling[9]. A rapid cooling rate helps to promote finer precipitation of Nb(C,N), ferrite grain refinement and acicular ferrite formation. The latter is preferred for a low ratio of yield strength to ultimate tensile strength[4], and it also avoids the development of any pearlite in the microstructure. A rapid cooling rate of 47 $°Cs^{-1}$could be achieved in the cooling box by using an aqueous solution of 10% NaCl for alloys #1 to #5 while a rate of 39 $°Cs^{-1}$could be obtained for the Mo-free alloy #6.

6.7.2.5 Simulation of coiling after laboratory hot rolling

The coiling temperature will influence the effectiveness of Nb-carbonitride but especially V(C,N) precipitation in the ferrite, thus controlling precipitation strengthening of these steels. If the coiling temperature is high, the precipitates will become coarser during coiling. A coiling temperature of 600 °C was selected for the study of these alloys as this was also the temperature used in the past by Mittal Steel before they recently lowered it to 575 ºC. After reaching 600 °C in the cooling box, the small plates were placed in a furnace at 600 °C until the temperature became

uniform throughout the plate. Thereafter they were well insulated for 24 hours using a generous covering of vermiculite for a slow cool simulating the actual coiling process in the plant.

6.7.2.6 Hot-rolling process curve

The hot-rolling process schedule is illustrated schematically in figure 6.12. The symbols R and F in the figure refer to the rough and finishing passes, respectively,

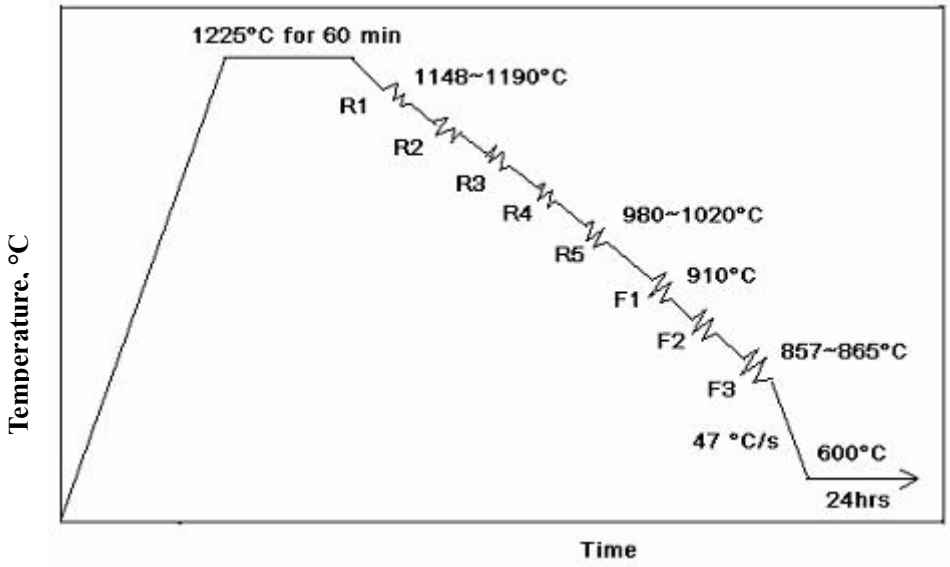

Figure 6.12 Schematic schedule of the hot rolling process on the experimental alloys.

6.8 The identification of acicular ferrite

The optimum microstructure of line pipe steels appears to be one that contains acicular ferrite and some polygonal ferrite. Acicular ferrite is very different from polygonal ferrite and bainitic ferrite. Polygonal ferrite, as the name implies, has polygonal boundaries with a carbon concentration in the ferrite that is almost uniform together with a lower dislocation density. Acicular ferrite, on the other hand, is characterised by fine non-equiaxed or interwoven nonparallel ferrite laths, which have various grain sizes and are arranged in a random manner[78]. Some M/A (martensite/austenite) islands and a high density of dislocations in-between the AF are common[11]. The carbon content in the M/A islands is higher than that in the surrounding matrix and accordingly, these islands are carbon-enriched

martensite/austenite islands whose formation may be attributed to the partitioning of carbon during the transformation to acicular ferrite and the post-transformation of carbon-enriched austenite. During accelerated cooling followed by the coiling process, part of the carbon-enriched austenite transforms to martensite and the remaining austenite will coexist with the martensite[73]. The accepted transformation model of acicular ferrite is a mix of diffusion and shear transformation[4,9,11,43].

Acicular ferrite contributes to a low yield strength and a higher tensile strength due to the lower carbon in the matrix and the M/A islands having a high density of dislocations and this, therefore, leads to a lower YS/UTS ratio. It was found initially that it was easy to confuse acicular ferrite with polygonal ferrite under an optical microscope when samples were etched in 2% Nital because the grain boundaries between them do not become clearly etched. Therefore, one of the key aspects of the experimental techniques in this study was how to distinguish between acicular ferrite and polygonal ferrite in low carbon, Nb-Ti micro-alloyed steels. Various techniques were initially attempted to identify the acicular ferrite, including the use of optical microscopy, Scanning Electron Microscopy (SEM), Transmission Electron Microscopy (TEM) using carbon extraction replicas with and without shadowing and finally, thin foil TEM samples.

6.8.1 Observation with optical microscopy and by SEM

Samples taken after hot rolling that were etched in a 2% Nital solution, were examined with an Olympus PMG3 optical microscope, both JEOL 5800LV and 6000F high resolution SEM, respectively. Acicular ferrite could not be distinguished from polygonal ferrite on the micrographs after etching with a light (5 seconds) or a deep etch (up to 120 seconds) under the optical microscope and SEM.

6.8.2 Observation of replicas by TEM

6.8.2.1 Preparing replicas without shadowing

Firstly, the polished samples were deeply etched from 30 to 60 seconds in a 2% Nital solution and thoroughly washed to remove all loose etching debris from the surface. Carbon coating was done under vacuum on the etched surface of the samples and the coating separated from the sample's surface in a mixture of 7 ml nitric acid and 75 ml ethanol before floating-off in distilled water.

6.8.2.2 Preparing shadowed carbon extraction replicas

The etched surface of the samples was first shadowed through vacuum evaporation with a gold-palladium alloy before the vertical deposition of carbon. Deep etching from 30 to 60 seconds was employed before the shadowing and the shadowing angle with respect to the surface was varied from 20° to 40°. The carbon was then coated vertically onto the shadowed layer. The technique used for separating the carbon film from the sample was the same as described above for the replicas without shadowing.

6.8.3 Thin foil TEM samples

Thin foil samples were used to further distinguish between acicular ferrite and polygonal ferrite and to also validate the results of the shadowed replicas in the TEM. Thin slices of material were cut by electro-discharge in a wire-cutting machine in order to reduce any adverse effect of deformation on the dislocation density in the samples that could have formed from mechanical cutting. The disc size was 3 mm in diameter and 0.6 mm in thickness and the procedure for preparing the thin foil samples was as follows:

- The original cylinder of material with dimensions of 3 mm diameter and 15 mm length was machined in a lathe;
- Five discs of 3 mm diameter and 0.6 mm thickness were cut from the cylinder with the electro-discharge wire-machine;
- The disc samples were carefully and lightly polished to between 50 to 80 μm

in thickness on fine grinding paper;

- The final thinning was done by electro-polishing with a solution of 1.25 l acetic acid, 0.08 l perchloric acid and 0.7 g chromium oxide at 25 °C.

All samples for replicas and thin foils were examined in a Philips CM200 TEM, operated at 60 or 200 KV, respectively.

6.9 Test of subsize samples on the Gleeble with various cooling rates, coiling temperatures and prior deformation

In order to study how some parameters of the controlled hot rolling process influence the YS/UTS ratio of steels, a series of experiments were planned. These parameters include cooling rates, coiling temperatures and deformation in the austenite.

The cooling rate after hot rolling has a strong effect on the fraction of acicular ferrite in Nb-Ti micro-alloyed steels and particularly, accelerated cooling after finish rolling helps to increase the volume fraction of acicular ferrite which may, in turn, influence the YS/UTS ratio. The coiling process controls the precipitation of particles in the matrix of these steels which affects dispersion hardening. The reduction during hot rolling also has an effect on the CCT diagram of these steels as well. A series of tests were designed for this purpose.

6.9.1 Hot rolling plates for Gleeble samples

Alloys #3 and #6 were selected for these tests. Casts of these alloys, firstly, were hot rolled to 6 mm thickness (the parameters of the hot rolling for plates are shown in Appendix H). Two types of preliminary samples were machined: the first type A to a rectangular size of 6 ×10 × 100 mm was used to study the effect of cooling rates and coiling temperature without deformation (figure 6.13-(a)), while the other type B shown schematically in figure 6.13-(b), was used to study the effect of prior compression in austenite, from there the shorter gauge length. At this stage, the gauge

lengths had not been machined into the rectangular samples, hence their being called "preliminary".

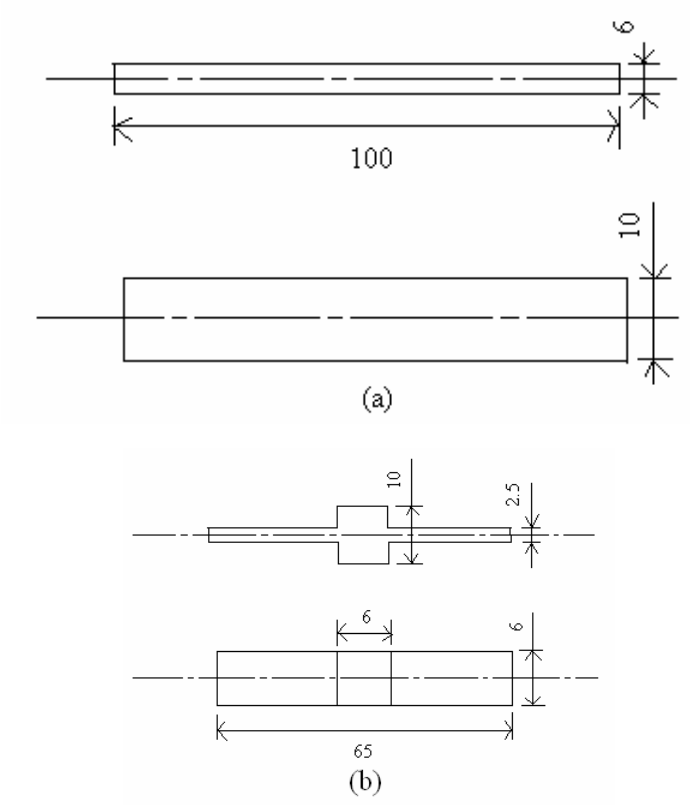

Figure 6.13 Preliminary samples on the Gleeble of (a) type A and (b) type B

6.9.2 Tests on the Gleeble

The first two groups of type A samples were tested at different cooling rates after austenitisation in which the cooling rates ranged from 1 to 51 ºCs^{-1} for the Mo-free alloy #6 (sample #A124) and 1 to 54 ºCs^{-1} for the 0.09% Mo alloy #3 (sample #AF3F). The process graph is shown schematically in figure 6.14.

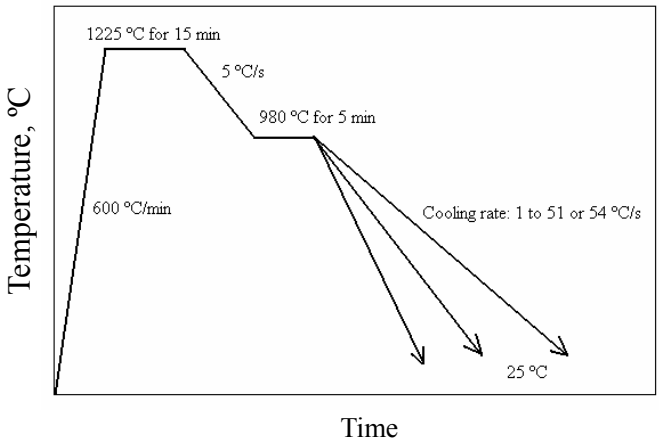

Figure 6.14 Graph of the heating and cooling process on the Gleeble for samples #A124 (the Mo-free alloy #6) and sample #AF3F (the 0.09% Mo alloy #3).

The second two groups of type A samples were subjected to a 60 minutes coiling simulation at 575 (sample #B113) and 600 ºC (sample #A113) for the Mo-free alloy #6, respectively, after cooling in Gleeble. The process graphs are illustrated schematically in figures 6.15.

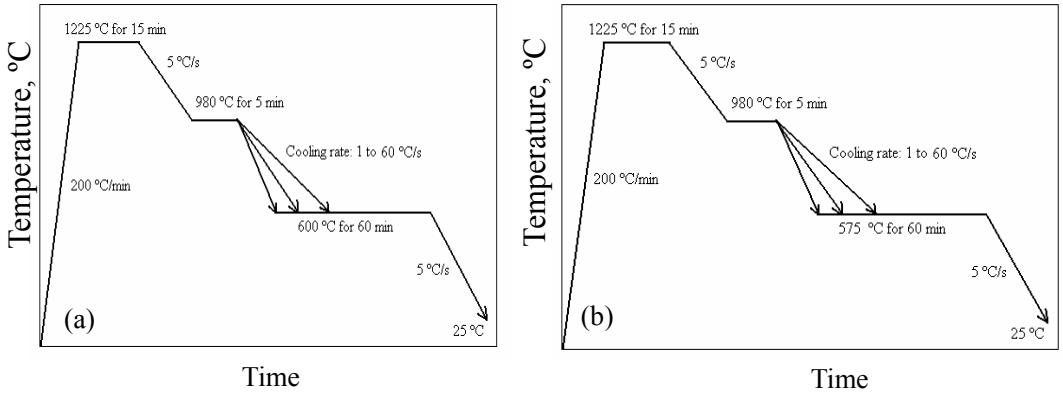

Figure 6.15 Graphs of the heating and cooling cycles in the Gleeble on the Mo-free alloy #6 for samples (a) #A113 and (b) #B113.

The last group, which consisted of type B samples (sample #TEN06 from the Mo-free alloy #6) was tested on the Gleeble with a prior 45% reduction in the austenite (only 33% reduction below the T_{nr}) before cooling and coiling simulation at 575 ºC for 60 minutes. Figure 6.16 shows the test process.

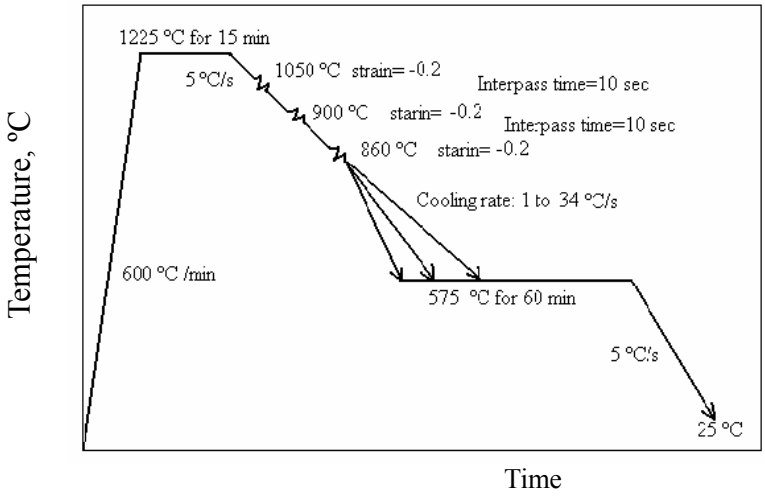

Figure 6.16 Graph of heating, cooling and deformation process in the Gleeble for sample #TEN06 (the Mo-free alloy #6).

6.9.3 Tensile tests

All of these rectangular and preliminary samples that were subjected to the above tests on the Gleeble, were thereafter machined with their gauge lengths to subsize tensile samples of type A (see figure 6.17-(a)) for the tensile test which was done on an INSTRON-8500 Digital Control tensile testing machine for the first four groups of samples and the type B (see figure 6.17-(b)) on a smaller instrumented Hounsfield tensile testing machine.

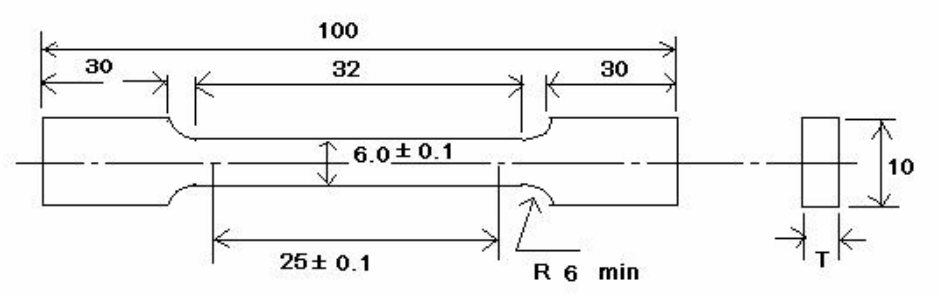

(a)

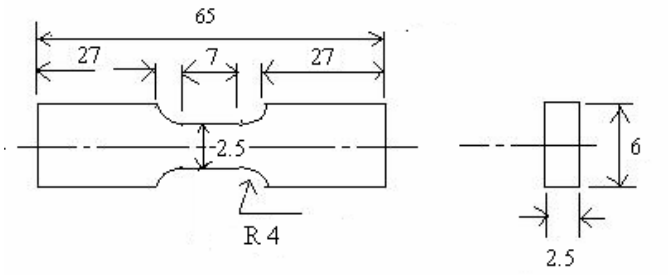

(b)

Figure 6.17 Tensile test samples of (a) type A and (b) type B. T is original thickness of the plates and 6 mm for the as-rolled alloy and the Gleeble samples, respectively.

6.10 Test of mechanical properties on the as-hot rolled alloys

The specimens for the tensile tests from the hot rolled plates were cut from the middle of the rolled plates in the longitudinal and transverse directions and were machined to the subsize tensile of type A (see figure 6.17-(a)). The tensile tests were carried out at room temperature on an INSTRON-8500 Digital Control tensile testing machine with an initial cross-head speed of 0.25 mm min^{-1} until the elongation of 0.5 mm was reached and then a second cross-head speed of 2 mm min^{-1} thereafter.